AGU PUBLICATIONS

Geophysical Research Letters

RESEARCH LETTER
10.1002/2016GL071845

Key Points:
- A decade of GPS measurements across the Andes image the megathrust seismic cycle before and between two great earthquakes in Chile
- Enhanced shear stress after a great earthquake drives transient super-interseismic phase in adjacent megathrust segments
- Increased plate locking and super-interseismic strain rates after the 2010 earthquake (*M*8.8) possibly triggered the 2015 event (*M*8.3)

Supporting Information:
- Supporting Information S1
- Movie S1
- Data Set S1
- Data Set S2
- Data Set S3

Correspondence to:
D. Melnick,
daniel.melnick@uach.cl

Citation:
Melnick, D., M. Moreno, J. Quinteros, J. C. Baez, Z. Deng, S. Li, and O. Oncken (2017), The super-interseismic phase of the megathrust earthquake cycle in Chile, *Geophys. Res. Lett.*, *44*, 784–791, doi:10.1002/2016GL071845.

Received 22 NOV 2016
Accepted 9 JAN 2017
Accepted article online 13 JAN 2017
Published online 27 JAN 2017

The super-interseismic phase of the megathrust earthquake cycle in Chile

Daniel Melnick[1,2], Marcos Moreno[3], Javier Quinteros[3], Juan Carlos Baez[4], Zhiguo Deng[3], Shaoyang Li[3], and Onno Oncken[3]

[1]Institute of Earth and Environmental Sciences, University of Potsdam, Potsdam, Germany, [2]Instituto de Ciencias de la Tierra, TAQUACH, Universidad Austral de Chile, Valdivia, Chile, [3]GFZ Helmholtz Centre Potsdam, Potsdam, Germany, [4]Centro Sismológico National, Universidad de Chile, Santiago, Chile

Abstract Along a subduction zone, great megathrust earthquakes recur either after long seismic gaps lasting several decades to centuries or over much shorter periods lasting hours to a few years when cascading successions of earthquakes rupture nearby segments of the fault. We analyze a decade of continuous Global Positioning System observations along the South American continent to estimate changes in deformation rates between the 2010 Maule (*M*8.8) and 2015 Illapel (*M*8.3) Chilean earthquakes. We find that surface velocities increased after the 2010 earthquake, in response to continental-scale viscoelastic mantle relaxation and to regional-scale increased degree of interplate locking. We propose that increased locking occurs transiently during a super-interseismic phase in segments adjacent to a megathrust rupture, responding to bending of both plates caused by coseismic slip and subsequent afterslip. Enhanced strain rates during a super-interseismic phase may therefore bring a megathrust segment closer to failure and possibly triggered the 2015 event.

1. Introduction

It has been long recognized that the timing of great megathrust earthquakes along a particular subduction zone is bimodal [e.g., *Anderson*, 1975; *Mogi*, 1968; *Satake and Atwater*, 2007]. For example, the giant 2004 Sumatra earthquake (*M*9.2) was preceded by a long seismic gap lasting several centuries and followed in a decade by three great earthquakes (*M*7.9–8.6) that ruptured nearby segments of the megathrust [e.g., *Lay*, 2015]. A similar pattern is suggested at millennial timescale by paleoseismic records showing supercycles characterized by earthquake clusters separated by protracted periods of relative quiescence [*Sieh et al.*, 2008]. The loading and triggering mechanisms of supercycle clusters remain poorly understood, mostly due to the paucity of geodetic time series extending before and between subsequent great earthquakes to detect and map changes in deformation rates. Models able to reproduce such changes may provide valuable information into Earth's rheology and the physical behavior of fault systems in the wake of great seismic events.

Shortly after the advent of plate tectonics, *Anderson* [1975] associated increased shear stresses caused by a transient acceleration in plate convergence rate after the first gap-closing event (i.e., 2004 Sumatra, 2010 Chile, and 2011 Japan) with the bimodal recurrence of megathrust earthquakes. However, his pioneering conceptual model was superseded by a range of popular mechanisms explaining megathrust earthquake triggering, including static stress transfer in the near field [e.g., *Lin and Stein*, 2004], changes in pore-fluid pressure [e.g., *Hughes et al.*, 2010], dynamic triggering in the far field [e.g., *Freed*, 2005], and transmission of viscous stresses in the mantle [e.g., *Klein et al.*, 2016; *Ruiz et al.*, 2016; *Wang et al.*, 2012]. The applied mechanism usually depends on data availability and extent of the region of interest and has not always been unambiguous. For example, the 2011 Tohoku earthquake (*M*9.1) was preceded and followed by changes in surface velocities, which have been associated with two contrasting processes: acceleration of shortening rates across the plate-boundary fault [*Heki and Mitsui*, 2013] and viscous relaxation of the oceanic and continental mantles [*Hu et al.*, 2016; *Sun et al.*, 2014; *Tomita et al.*, 2015]. To address this problem and attempt to isolate both processes—elastic versus viscous stress transfer—we focus on central Chile where great earthquakes occurred on nearby (but not adjacent) megathrust segments in 2010 and 2015. We compare decadal-scale changes in surface deformation throughout the Andes with numerical experiments to explore the relation between the 2010 and 2015 earthquakes and gain insight on the mechanisms associated with cascading earthquake sequences. We propose that the 2010 earthquake caused a super-interseismic phase of enhanced strain accumulation in the adjacent segments, which may have triggered the 2015 event.

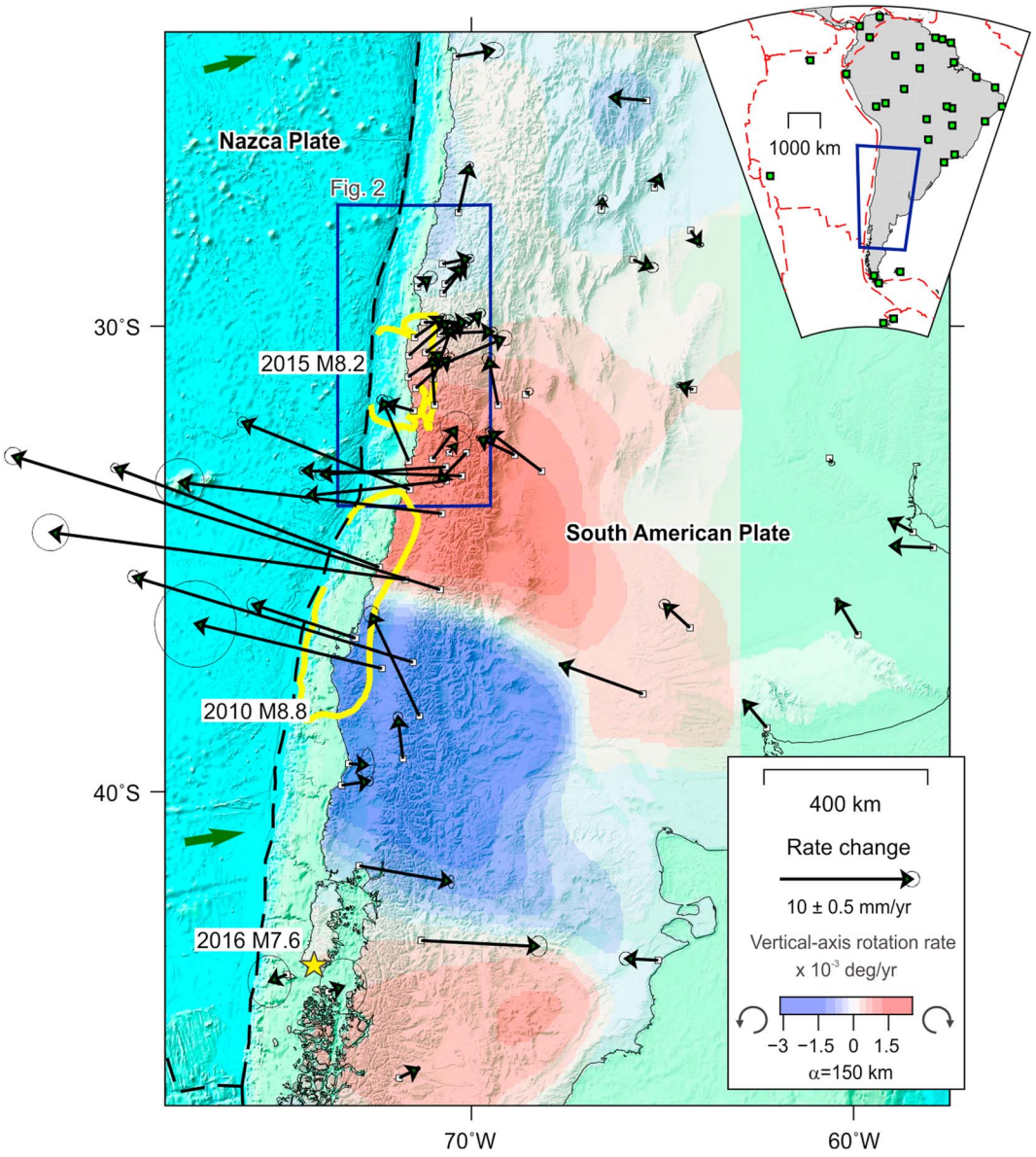

Figure 1. Changes in GPS velocities after the 2010 Maule earthquake. Arrows show the linear component of surface velocities estimated from continuous GPS stations with respect to the pre-2010 velocity. Ellipses indicate the 50% confident level. Thick yellow lines show 1 m contour of the 2010 and 2015 earthquakes [*Moreno et al.*, 2012; *Tilmann et al.*, 2016]. Color coding shows vertical-axis rotation rate estimated using inverse distant weighting (details in the supporting information); red and blue indicate clockwise and counterclockwise rotations, respectively. Note symmetric rotation about the center of the 2010 rupture. The dark blue box shows the Illapel earthquake area in Figure 2. The yellow star shows the epicenter of the 2016 earthquake from the National Earthquake Information Center catalogue. Time series and trajectory models can be found in Figure S2 in the supporting information.

2. Seismotectonic Setting

The Andean megathrust accounts for convergence of the Nazca and South American plates at 66 mm/yr (Figure 1). Kinematic models suggest that the plate interface is mostly locked during long interseismic periods and slips during great earthquakes and the subsequent afterslip [e.g., *Moreno et al.*, 2010; *Wang et al.*, 2012; *Wesson et al.*, 2015]. The 2010 Maule earthquake (*M*8.8) ruptured ~500 km of the Andean megathrust in a region of high degree of preseismic plate locking [*Moreno et al.*, 2010]—the ratio between interseismic slip deficit rate or backslip rate and plate convergence velocity. The 2010 earthquake resembled its predecessor in 1835, documented by FitzRoy and Darwin, closing a 175 year long seismic gap [*Melnick et al.*, 2012; *Wesson et al.*, 2015]. In

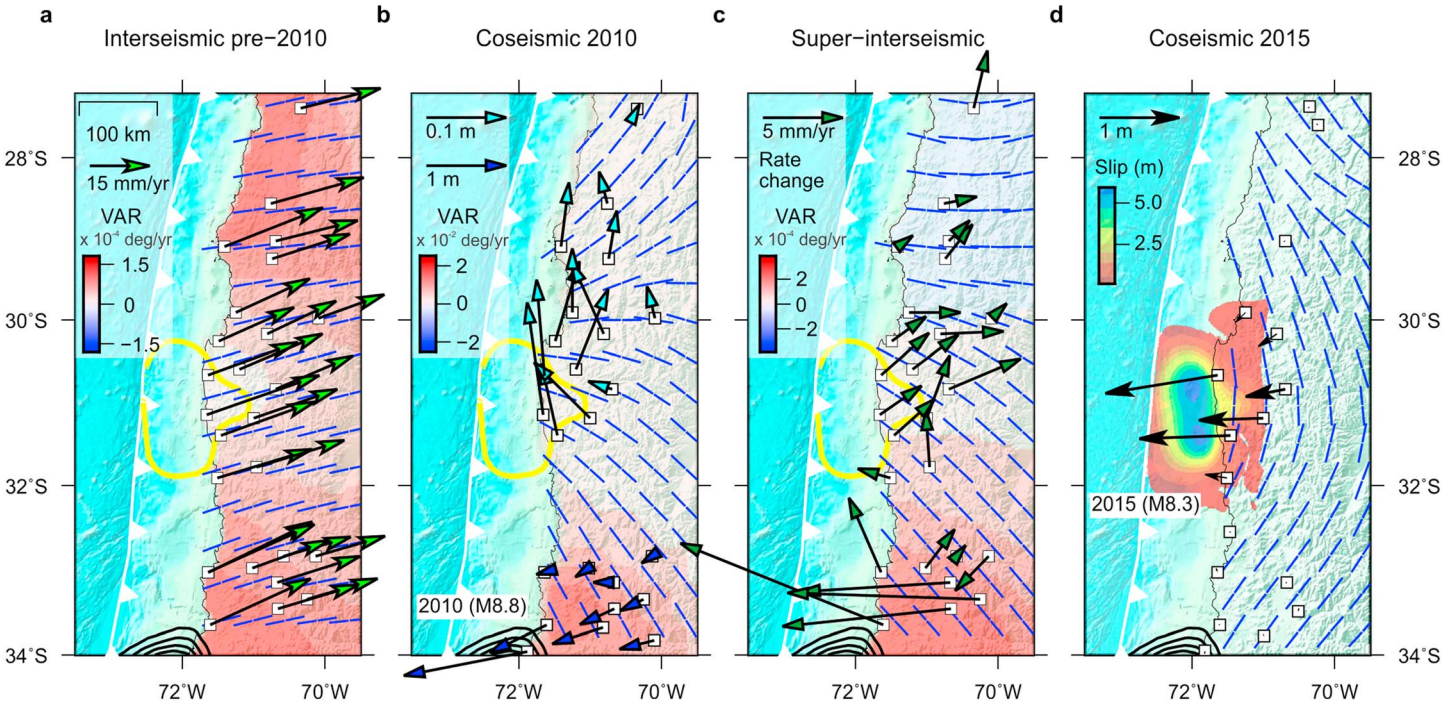

Figure 2. Deformation during the 2010–2015 earthquake cycle. (a) Pre-2010 velocities from continuous GPS in a stable South American reference frame (Methods in the supporting information). Error ellipses have been omitted for clarity and can be found in Table S1. Colors show vertical-axis rotation rate; blue lines show infinitesimal shortening axes. (b) Coseismic GPS displacements during the 2010 earthquake [*Moreno et al.*, 2012; *Vigny et al.*, 2011]. (c) Linear post-2010 earthquake velocities with respect to their pre-2010 velocities. (d) Static coseismic displacements and 1 m slip contours of the *M*8.3 Illapel main shock [*Tilmann et al.*, 2016].

2015, the Illapel earthquake (*M*8.3) ruptured north of the 2010 event (Figure 2), also in an area characterized by a high degree of preseismic plate locking (Figure 3) [*Tilmann et al.*, 2016], but where the previous earthquake occurred in 1943 and had a lesser magnitude of 7.9 [*Beck et al.*, 1998]. The Illapel earthquake occurred ~200 km north of the northern edge of the Maule rupture (Figure 1), in an area affected by post-2010 transient deformation associated with viscoelastic relaxation of the continental mantle [*Klein et al.*, 2016]. These rapid transient motions lasted for at least ~2 years and affected mostly the margin-parallel component of GPS displacements, manifested in faster northward motion with respect to pre-earthquake velocity [*Ruiz et al.*, 2016].

In central Chile, earthquake doublets breaking nearby megathrust segments, separated by long interseismic periods (i.e., seismic gaps), occurred in 1570–1575, 1647–1657, 1730–1751, 1822–1835, and 1906–1922 (Figure S1 in the supporting information). These were all great ($M > 8$) earthquakes that generated transpacific tsunamis [*Beck et al.*, 1998; *Cisternas et al.*, 2005; *Cisternas et al.*, 2012; *Lomnitz*, 2004; *Udías et al.*, 2012].

3. Background and Modeling Strategies

In order to quantify velocity changes associated with the plate-boundary earthquake cycle, we used decadal-scale GPS measurements obtained from continuous stations surrounding the 2010 earthquake rupture zone, at continental scale (Figures 1 and S1–S4). First, we evaluated the stability of the reference frame by analyzing 32 far-field sites spanning ~8000 km, located between the Antarctic Peninsula, the Caribbean, and Eastern Island (Figure S4), using the Standard Linear Trajectory Model [*Bevis and Brown*, 2014]. Then, we estimated velocity changes at an additional 60 GPS stations surrounding the 2010 rupture zone across the Andes (Figure 1), using the Extended Linear Trajectory Model [*Bevis and Brown*, 2014]. This extended model accounts for postseismic transients commonly observed in middle- and near-field GPS stations (at distances $< \sim 10^3$ km from the rupture limits). An extensive description of GPS processing and trajectory modeling may be found in the supporting information [*Angermann et al.*, 1997; *Altamimi et al.*, 2011; *Loveless and Meade*, 2016; *Weiss et al.*, 2016; *Blewit*, 2016].

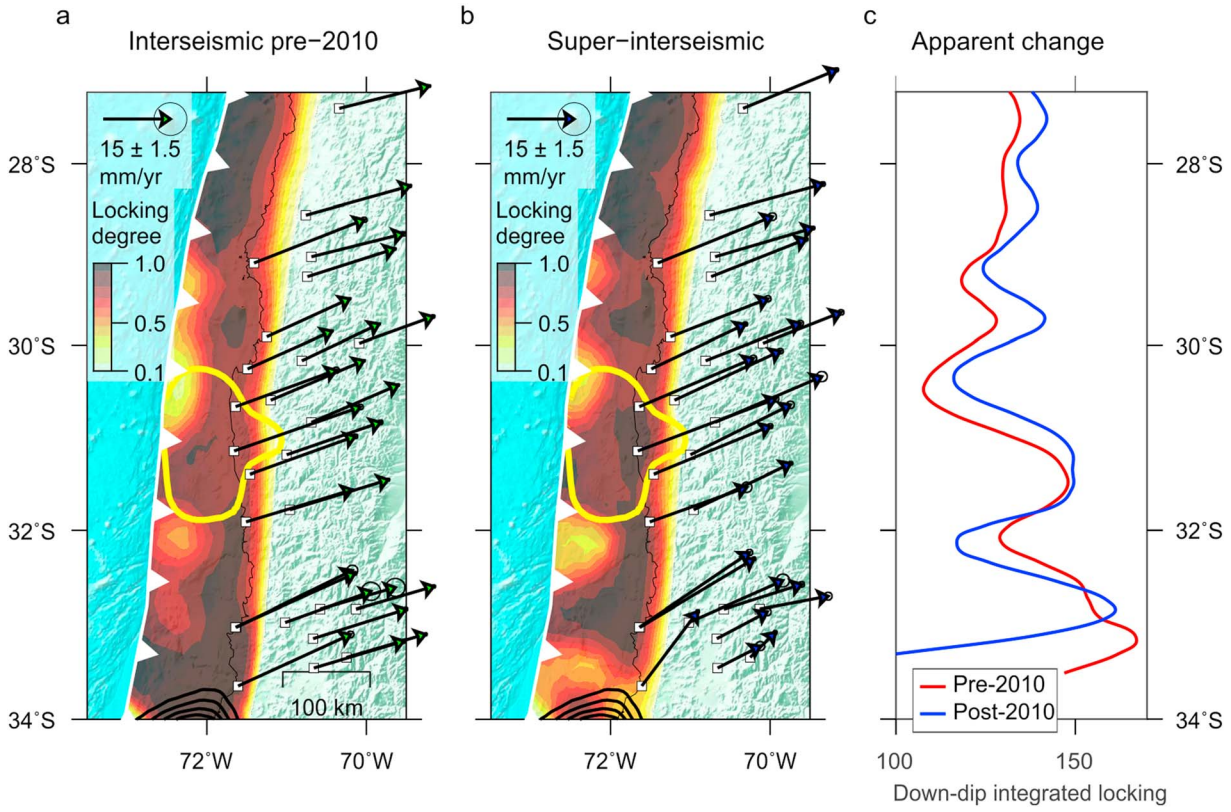

Figure 3. Plate locking before and after the 2010 earthquake. (a) Degree of interseismic plate locking expressed as a fraction of plate convergence rate before the 2010 earthquake (Methods in the supporting information). Error ellipses represent the 95% confident level. Black and yellow contours denote 1 m slip contours during the 2010 and 2015 earthquakes [*Moreno et al*., 2012; *Tilmann et al*., 2016]. (b) Plate locking estimated using linear GPS velocities between the 2010 and 2015 earthquakes. (c) Integrated downdip locking rate from the pre-2010 and post-2010 models. Note decrease in locking adjacent to the 2010 rupture edge likely associated with afterslip and increase throughout the 2015 rupture zone and farther north.

Postseismic transients observed in GPS time series after great earthquakes have been commonly associated with afterslip and viscous relaxation of the oceanic and continental mantles [e.g., *Hu et al*., 2016; *Wang et al*., 2012]. The former process usually takes place within the rupture zone and its immediate vicinity with a duration of a few years [e.g., *Bedford et al*., 2013] and might be distinguished from the latter by a combination of GPS time-series analysis and numerical modeling [e.g., *Bedford et al*., 2016]. Viscoelastic relaxation of the mantle is reflected in a transient phase of fast surface deformation that decays gradually with time as a function of amount of coseismic slip, distance to the rupture edges, and mantle viscosity and geometry [e.g., *Klein et al*., 2016; *Moreno et al*., 2011; *Wang et al*., 2012]. In an attempt to separate the secular elastic deformation related to plate-boundary locking from the viscous contribution in the postseismic deformation signal, we analyzed the GPS time series and isolated components associated with linear, logarithmic, and seasonal trends while taking into account sporadic jumps caused by local earthquakes or instrumental changes (details in the supporting information).

Our analysis of 60 GPS stations surrounding the 2010 earthquake showed that the logarithmic contribution is much larger for the north component of GPS displacements (Figure S3), resulting in apparent margin-parallel accelerations along the 2015 earthquake region [*Ruiz et al*., 2016]. Thus, in order to account for such effects, we filtered-out the transient post-2010 logarithmic components from the GPS time series (Figures S2–S4 and Movie S1) and analyzed the pre-earthquake and post-earthquake linear components, which may be directly compared with each other to estimate changes in interseismic strain accumulation (Figure 2) and the apparent degree of plate locking (Figure 3). We estimated the velocity gradient tensor from linear GPS velocities for pre-2010 and post-2010 earthquake epochs and extracted the principal axes of infinitesimal shortening and vertical-axis rotation rates using an inverse distance weighted interpolation approach [*Allmendinger et al*., 2007, 2011] (details in the supporting information). The degree of interseismic plate locking was estimated

using the geometry of the plate interface estimated from geophysical images and following the approach of *Moreno et al*. [2011] (details in the supporting information).

Displacements and stress changes associated with the 2010 earthquake at continental scale are inferred using a 3-D thermomechanical approach (details in the supporting information) using the SLIM3D code [*Popov and Sobolev*, 2008]. The model setup is based on a previous study of Andean deformation [*Quinteros and Sobolev*, 2013] and is not intended to reproduce the GPS displacements or velocities, but to gain insight into the earthquake-cycle processes and provide a conceptual framework to evaluate the research hypotheses. Experiments simulate the 2010 earthquake by decreasing the coefficient of friction of the megathrust over a 500 km region, which resulted in a ~10 MPa stress drop for our preferred model, similar to estimates from force balance modeling [e.g., *Luttrell et al*., 2011]. We performed experiments with different drops in friction coefficient (Table S3), finding similar patterns in surface rate-changes and vertical-axis rotations (Figures 4a and 4b), with variations in the amplitude and wavelength.

4. Deformation Patterns Before and After the 2010 Maule Earthquake

Great megathrust earthquake such as the 2010 Maule event commonly cause deformation at continental scale [*Vigny et al*., 2011] and may cause apparent changes in secular velocities if transient effects are not taken into account at GPS sites used to estimate the reference frame [*Bevis and Brown*, 2014; *Sánchez and Drewes*, 2016; *Weiss et al*., 2016]. We attempt to estimate the amplitude of such bias from the distribution of velocity changes after the 2010 earthquake at far-field sites across South America (Figure S4). These sites experienced a mean rate-change increase of 1.0 ± 0.6 mm/yr, which we infer to represent the level of background noise. Therefore, higher rate-changes most likely resulted from variations in tectonic stresses associated with the earthquake cycle.

Previous studies have shown that in the 2015 earthquake region, the phase of rapid post-2010 decay lasted for at least ~2 years after the earthquake [*Klein et al*., 2016; *Ruiz et al*., 2016]. Indeed, our analysis of GPS time series (Figure S2) shows that after ~2 years following the 2010 earthquake, displacements tend to exhibit secular linear trends typical of interseismic plate locking. The rapid phase of post-2010 deformation is manifested in a rapid margin-parallel motion evident in the north component of GPS time series (Figure S2a) and much larger amplitude of the logarithmic trend (Figure S3). In contrast, the linear component of GPS time series (Methods in the supporting information) shows a predominant increase in the margin-normal component (Figure S2b). Indeed, linear components dominate the amplitude of GPS displacements with respect to the logarithmic contribution (Figure S3). Post-2010 linear GPS velocities (Figures 1 and 2) reveal post-2010 deformation patterns that are opposite to motion of crustal blocks and back-arc shortening [*Wang et al*., 2007], likely associated with stress changes along the megathrust.

Velocities estimated from the linear components of post-2010 displacements with respect to their pre-2010 velocity (the rate-change) show consistent patterns of gear-train vertical-axis rotations at continental scale (Figure 1). Interestingly, the 2015 rupture occurred at the convergent junction of two vertical-axis rotation gears, where the orientation of the principal axes of infinitesimal strain changed during the past decade. Before the 2010 earthquake, shortening axes were parallel to the plate convergence direction (Figure 2a) as expected from interseismic locking. During the 2010 earthquake, shortening axes rotated surrounding its rupture zone but remained at high angle to the margin within region affected by the 2015 earthquake (Figure 2b), implying a local increase in upper plate strain rates. Shortening axes calculated from the rate-change vectors also have similar orientations (Figure 2c), implying that upper-plate contraction further augmented between the 2010 and 2015 earthquakes. This increase is also reflected in a ~20% rise in the degree of apparent interseismic plate locking within the 2015 rupture zone (Figure 3); see supporting information [*Masterlark*, 2003; *Bürgmann et al*., 2005; *Tassara and Echaurren*, 2012; *Béjar-Pizzaro et al*., 2013; *Melnick*, 2016].

Results of the 3-D modeling experiments show a transient increase in the shortening rate across the plate boundary fault in response to coseismic and postseismic fault slip during and after the 2010 Maule earthquake rupture. Our preferred model predicts an increase in megathrust shear stresses of 6.3% and 5.8% at 110 and 70 km from the 2010 rupture edges, respectively (Figure 4c). Interestingly, the predicted stress changes are slightly higher farther away from the rupture edges, forming a spatial pattern that is similar to the gap between the 2010 and 2015 ruptures (Figure 1).

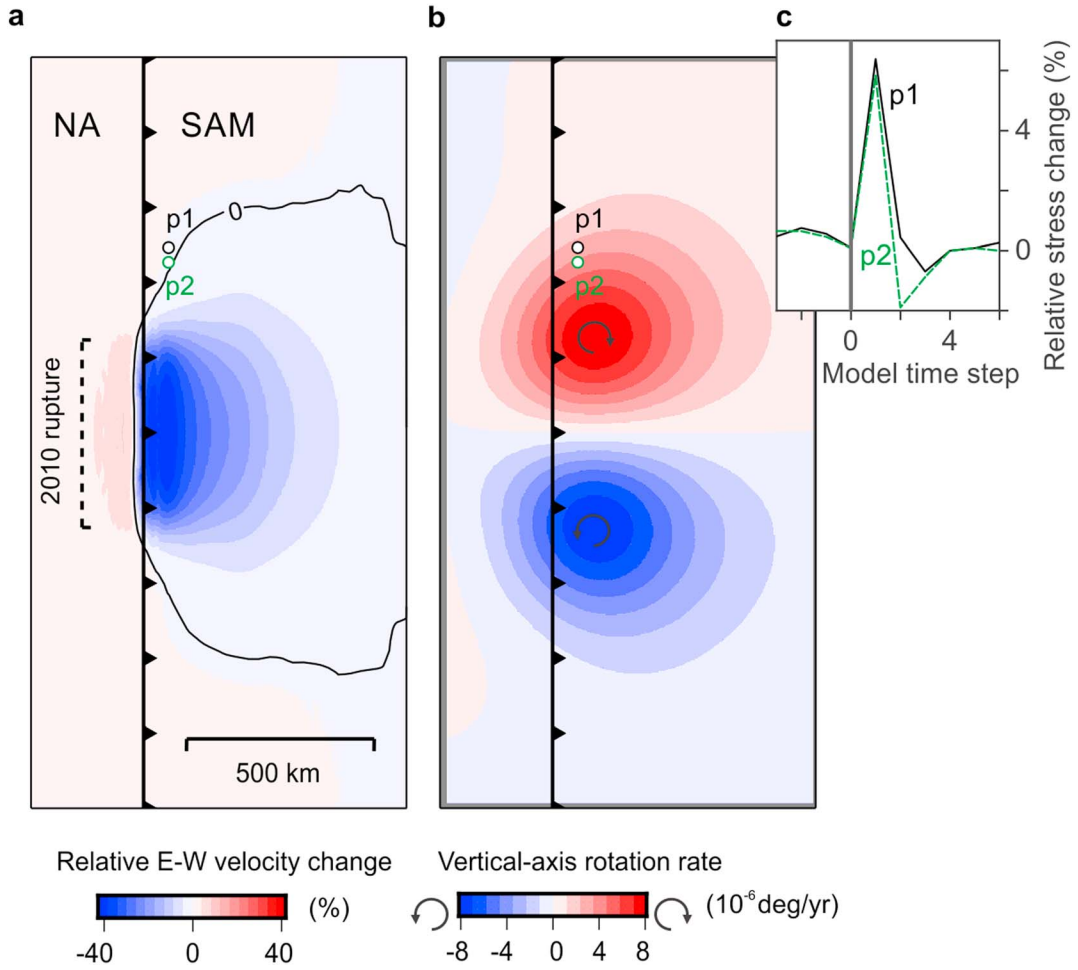

Figure 4. Simulation of deformation during and after the 2010 earthquake. (a) E-W velocity changes after the earthquake from our preferred simulation (model 3 in Table S3). Note increase in velocities of the Nazca (NA) and South American (SAM) plates with opposite sense during super-interseismic accelerated shortening across the plate-boundary fault. Dots mark the two locations of estimated stress changes. (b) Vertical-axis rotation rate estimated from the modeled velocity changes using the same parameters as in Figure 1. Note symmetric gear-like pattern. (c) Temporal evolution of plate-boundary shear stress estimated on the megathrust at points p1 and p2. Stress changes from different model setups can be found in Figure S9.

5. Discussion and Implications for Cascading Earthquake Sequences

Our modeling experiments suggest that the elastic response of both oceanic and continental plates, caused by coseismic and postseismic fault slip, resulted in increased shortening rate across the megathrust and in higher shear stresses on adjacent segments of the megathrust. We propose that such increased shear stresses cause an apparent higher degree of plate locking constituting a super-interseismic phase. The super-interseismic phase that started during the 2010 earthquake is characterized by faster surface velocities and shortening rates surrounding the rupture zone, with a symmetric pattern of vertical-axis rotation (Figures 1 and 2). Higher plate locking during the super-interseismic phase will increase upper plate strain accumulation rates and may bring a particular segment of the megathrust closer to failure. We propose that the 2015 event was indeed triggered by such an increase in megathrust shear stresses throughout the super-interseismic phase that started during the 2010 earthquake. Therefore, the 2015 event likely closed the super-interseismic phase locally, while it still prevails between 27.5°S and 29.5°S and south of 40°S (Figures 1 and 3). This southern region is characterized by heterogeneous locking after the giant 1960 (*M*9.5) earthquake [*Moreno et al.*, 2011] and thus may not be yet mature for another great earthquake. However, on 25 December 2016, a *M*7.6 earthquake occurred at 43.4°S (star in Figure 1) in the area of increased margin-normal velocities, possibly a response to the

super-interseismic phase. The 27.5–29.5°S, in turn, is characterized by a high degree of plate locking (Figure 3) and seismic gap since the 1922 earthquake (*M*8.3) and thus may generate another $M > 8$ earthquake anytime. The ~200 km gap between the 2010 and 2015 ruptures (Figure 1) likely resulted from a combination of the 2010 slip distribution, rigidity of both plates, and preseismic degree of locking.

After the 2011 Tohoku earthquake, seafloor geodesy measured a twofold increase in the velocity of the Pacific plate near the trench, inferred to result from viscous mantle flow [*Tomita et al*., 2015]. Our modeling experiments—that include viscous rheology—show accelerated shortening across the plate-boundary fault associated with regional-scale vertical-axis rotations and increased strain rates throughout the continent, which take place during the earthquake and throughout the subsequent super-interseismic phase. We propose that the elastic bending of both plates in response to megathrust coseismic slip and subsequent afterslip results in gear-train rotation patterns and changes in the strain field as those observed after the 2010 earthquake throughout the Andes, including the immediate and protracted increase in GPS velocities. These observations are difficult to account for by exclusively viscous processes because these act over much larger spatial scales with wavelengths of several hundreds of kilometers and smooth gradients. Because elastic strain is the main source of seismic energy, enhancing its accumulation during a super-interseismic phase will bring a particular fault segment closer to failure, increasing the probability of an imminent earthquake. Super-interseismic strain rates may thus trigger cascading earthquake sequences depending on the state of stress and plate locking of the nearby megathrust segments.

Enhanced super-interseismic strain rates may explain observations from different subduction zones, such as the sudden increase in interseismic velocities inferred from Sumatran corals between pairs of great earthquakes [*Meltzner et al*., 2015; *Philibosian et al*., 2014], the ~200 km long Mentawai gap between the 2004–2005 and 2007–2008 sequences of great earthquake in Sumatran [*Lay*, 2015], and multisegment ruptures during prehistoric sequences in Japan [e.g., *Garrett et al*., 2016], Alaska [e.g., *Shennan et al*., 2016], and Cascadia [e.g., *Nelson et al*., 2006]. The future challenge is gaining detailed insight on the processes controlling the duration of the super-interseismic phase and lag time between cascading earthquakes, which should be a function of coseismic slip during the first event, degree of interseismic plate locking, rheology and structure of the continental and oceanic plates, and transient mechanics of the megathrust.

Acknowledgments
We thank all institutions that made GPS data available in the frame of the IPOC Network (www.ipoc-network.org). D.M. and M.M. were supported by German Science Foundation (DFG) grants ME-3157/4-2 and MO-2310/3-1, respectively. J.Q. was supported by Helmholtz Association grant HIRG-0008. We thank Chris Vigny, Luce Fleitout, Raúl Madariaga, Sergio Ruiz, and Kelin Wang for fruitful discussions, Roland Bürgmann and Rob Wesson for comments on the manuscript, and Jack Loveless for his constructive review.

References

Allmendinger, R. W., R. Reilinger, and J. Loveless (2007), Strain and rotation rate from GPS in Tibet, Anatolia, and the Altiplano, *Tectonics*, *26*, TC3013, doi:10.1029/2006TC002030.

Allmendinger, R. W., N. Cardozo, and D. M. Fisher (2011), *Structural Geology Algorithms: Vectors and Tensors*, Cambridge Univ. Press, New York.

Altamimi, Z., X. Collilieux, and L. Métivier (2011), ITRF2008: An improved solution of the international terrestrial reference frame, *J. Geod.*, *85*(8), 457–473.

Anderson, D. L. (1975), Accelerated plate tectonics, *Science*, *187*(4181), 1077–1079.

Angermann, D., G. Baustert, R. Galas, and S. Zhu (1997), *EPOS. P. V3 (Earth Parameter & Orbit System): Software User Manual for GPS Data Processing*, Geoforschungszentrum, Potsdam.

Beck, S., S. Barrientos, E. Kausel, and M. Reyes (1998), Source characteristics of historic earthquakes along the central Chile subduction zone, *J. South Am. Earth Sci.*, *11*(2), 115–129.

Bedford, J., M. Moreno, J. C. Baez, D. Lange, F. Tilmann, M. Rosenau, O. Heidbach, O. Oncken, M. Bartsch, and A. Rietbrock (2013), A high-resolution, time-variable afterslip model for the 2010 Maule $M_w = 8.8$, Chile megathrust earthquake, *Earth Planet. Sci. Lett.*, *383*, 26–36.

Bedford, J., M. Moreno, S. Li, O. Oncken, J. C. Baez, M. Bevis, O. Heidbach, and D. Lange (2016), Separating simultaneous postseismic processes: An application of the postseismic straightening method to the Maule 2010 cGPSv, *J. Geophys. Res. Solid Earth*, *121*, 7618–7638, doi:10.1002/2016JB013093.

Béjar-Pizarro, M., A. Socquet, R. Armijo, D. Carrizo, J. Genrich, and M. Simons (2013), Andean structural control on interseismic coupling in the North Chile subduction zone, *Nat. Geosci.*, *6*(6), 462–467.

Bevis, M., and A. Brown (2014), Trajectory models and reference frames for crustal motion geodesy, *J. Geod.*, *88*(3), 283–311.

Blewit, G. (2016), GPS Networks Map from the Nevada Geodetic Laboratory, edited. [Available at http://geodesy.unr.edu/.]

Bürgmann, R., M. G. Kogan, G. M. Steblov, G. Hilley, V. E. Levin, and E. Apel (2005), Interseismic coupling and asperity distribution along the Kamchatka subduction zone, *J. Geophys. Res.*, *110*, B07405, doi:10.1029/2005JB003648.

Cisternas, M., B. F. Atwater, F. Torrejón, Y. Sawai, G. Machuca, M. Lagos, A. Eipert, C. Youlton, I. Salgado, and T. Kamataki (2005), Predecessors of the giant 1960 Chile earthquake, *Nature*, *437*(7057), 404–407.

Cisternas, M., F. Torrejón, and N. Gorigoitia (2012), Amending and complicating Chile's seismic catalog with the Santiago earthquake of 7 August 1580, *J. South Am. Earth Sci.*, *33*(1), 102–109.

Freed, A. M. (2005), Earthquake triggering by static, dynamic, and postseismic stress transfer, *Annu. Rev. Earth Planet. Sci.*, *33*, 335–367.

Garrett, E., O. Fujiwara, P. Garrett, V. M. Heyvaert, M. Shishikura, Y. Yokoyama, A. Hubert-Ferrari, H. Brückner, A. Nakamura, and M. De Batist (2016), A systematic review of geological evidence for Holocene earthquakes and tsunamis along the Nankai-Suruga Trough, Japan, *Earth Sci. Rev.*, *159*, 337–357.

Heki, K., and Y. Mitsui (2013), Accelerated pacific plate subduction following interplate thrust earthquakes at the Japan trench, *Earth Planet. Sci. Lett.*, *363*, 44–49.

Hu, Y., R. Bürgmann, N. Uchida, P. Banerjee, and J. T. Freymueller (2016), Stress-driven relaxation of heterogeneous upper mantle and time-dependent afterslip following the 2011 Tohoku earthquake, *J. Geophys. Res. Solid Earth*, *121*, 385–411, doi:10.1002/2015JB012508.
Hughes, K. L. H., T. Masterlark, and W. D. Mooney (2010), Poroelastic stress-triggering of the 2005 *M*8. 7 Nias earthquake by the 2004 *M*9.2 Sumatra–Andaman earthquake, *Earth Planet. Sci. Lett.*, *293*(3), 289–299.
Klein, E., L. Fleitout, C. Vigny, and J. D. Garaud (2016), Afterslip and viscoelastic relaxation model inferred from the large-scale post-seismic deformation following the 2010 M_w 8.8 Maule earthquake (Chile), *Geophys. J. Int.*, *205*(3), 1455–1472.
Lay, T. (2015), The surge of great earthquakes from 2004 to 2014, *Earth Planet. Sci. Lett.*, *409*, 133–146.
Lin, J., and R. S. Stein (2004), Stress triggering in thrust and subduction earthquakes and stress interaction between the southern San Andreas and nearby thrust and strike–slip faults, *J. Geophys. Res.*, *109*, B02303, doi:10.1029/2003JB002607.
Lomnitz, C. (2004), Major earthquakes of Chile: A historical survey, 1535–1960, *Seismol. Res. Lett.*, *75*(3), 368–378.
Loveless, J. P., and B. J. Meade (2016), Two decades of spatiotemporal variations in subduction zone coupling offshore Japan, *Earth Planet. Sci. Lett.*, *436*, 19–30.
Luttrell, K. M., X. Tong, D. T. Sandwell, B. A. Brooks, and M. G. Bevis (2011), Estimates of stress drop and crustal tectonic stress from the 27 February 2010 Maule, Chile, earthquake: Implications for fault strength, *J. Geophys. Res.*, *116*, B11401, doi:10.1029/2011JB008509.
Masterlark, T. (2003), Finite element model predictions of static deformation from dislocation sources in a subduction zone: Sensitivities to homogeneous, isotropic, Poisson-solid, and half-space assumptions, *J. Geophys. Res.*, *108*(B11), 2540, doi:10.1029/2002JB002296.
Melnick, D. (2016), Rise of the central Andean coast by earthquakes straddling the Moho, *Nat. Geosci.*, *9*(5), 401–407.
Melnick, D., M. Moreno, M. Cisternas, and A. Tassara (2012), Darwin seismic gap closed by the 2010 Maule earthquake, *Andean Geol.*, *39*(3), 558–563.
Meltzner, A. J., K. Sieh, H.-W. Chiang, C.-C. Wu, L. L. H. Tsang, C.-C. Shen, E. M. Hill, B. W. Suwargadi, D. H. Natawidjaja, and B. Philibosian (2015), Time-varying interseismic strain rates and similar seismic ruptures on the Nias–Simeulue patch of the Sunda megathrust, *Quat. Sci. Rev.*, *122*, 258–281.
Mogi, K. (1968), Sequential occurrences of recent great earthquakes, *J. Phys. Earth*, *16*(1), 30–36.
Moreno, M., M. Rosenau, and O. Oncken (2010), 2010 Maule earthquake slip correlates with pre-seismic locking of Andean subduction zone, *Nature*, *467*(7312), 198–202.
Moreno, M., D. Melnick, M. Rosenau, J. Bolte, J. Klotz, H. Echtler, J. Baez, K. Bataille, J. Chen, and M. Bevis (2011), Heterogeneous plate locking in the south-central Chile subduction zone: Building up the next great earthquake, *Earth Planet. Sci. Lett.*, *305*(3), 413–424.
Moreno, M., D. Melnick, M. Rosenau, J. Baez, J. Klotz, O. Oncken, A. Tassara, J. Chen, K. Bataille, and M. Bevis (2012), Toward understanding tectonic control on the M_w 8.8 2010 Maule Chile earthquake, *Earth Planet. Sci. Lett.*, *321*, 152–165.
Nelson, A. R., H. M. Kelsey, and R. C. Witter (2006), Great earthquakes of variable magnitude at the Cascadia subduction zone, *Quat. Res.*, *65*(3), 354–365.
Philibosian, B., K. Sieh, J.-P. Avouac, D. H. Natawidjaja, H.-W. Chiang, C.-C. Wu, H. Perfettini, C.-C. Shen, M. R. Daryono, and B. W. Suwargadi (2014), Rupture and variable coupling behavior of the Mentawai segment of the Sunda megathrust during the supercycle culmination of 1797 to 1833, *J. Geophys. Res. Solid Earth*, *119*, 7258–7287, doi:10.1002/2014JB011200.
Popov, A. A., and S. V. Sobolev (2008), SLIM3D: A tool for three-dimensional thermomechanical modeling of lithospheric deformation with elasto-visco-plastic rheology, *Phys. Earth Planet. Inter.*, *171*(1), 55–75.
Quinteros, J., and S. V. Sobolev (2013), Why has the Nazca plate slowed since the Neogene?, *Geology*, *41*(1), 31–34.
Ruiz, S., E. Klein, F. del Campo, E. Rivera, P. Poli, M. Metois, C. Vigny, J. C. Baez, G. Vargas, and F. Leyton (2016), The Seismic Sequence of the 16 September 2015 M_w 8.3 Illapel, Chile, Earthquake, *Seismol. Res. Lett.*, *87*(4), 789–799.
Sánchez, L., and H. Drewes (2016), Crustal deformation and surface kinematics after the 2010 earthquakes in Latin America, *J. Geodyn.*, *102*, 1–23.
Satake, K., and B. F. Atwater (2007), Long-term perspectives on giant earthquakes and tsunamis at subduction zones, *Annu. Rev. Earth Planet. Sci.*, *35*, 349–374.
Shennan, I., E. Garrett, and N. Barlow (2016), Detection limits of tidal-wetland sequences to identify variable rupture modes of megathrust earthquakes, *Quat. Sci. Rev.*, *150*, 1–30.
Sieh, K., D. H. Natawidjaja, A. J. Meltzner, C. C. Shen, H. Cheng, K. S. Li, B. W. Suwargadi, J. Galetzka, B. Philibosian, and R. L. Edwards (2008), Earthquake supercycles inferred from sea-level changes recorded in the corals of west Sumatra, *Science*, *322*(5908), 1674–1678.
Sun, T., K. Wang, T. Iinuma, R. Hino, J. He, H. Fujimoto, M. Kido, Y. Osada, S. Miura, and Y. Ohta (2014), Prevalence of viscoelastic relaxation after the 2011 Tohoku-oki earthquake, *Nature*, *514*(7520), 84–87.
Tassara, A., and A. Echaurren (2012), Anatomy of the Andean subduction zone: Three-dimensional density model upgraded and compared against global-scale models, *Geophys. J. Int.*, *189*(1), 161–168.
Tilmann, F., et al. (2016), The 2015 Illapel earthquake, central Chile: A type case for a characteristic earthquake?, *Geophys. Res. Lett.*, *43*, 574–583, doi:10.1002/2015GL066963.
Tomita, F., M. Kido, Y. Osada, R. Hino, Y. Ohta, and T. Iinuma (2015), First measurement of the displacement rate of the Pacific Plate near the Japan Trench after the 2011 Tohoku-Oki earthquake using GPS/acoustic technique, *Geophys. Res. Lett.*, *42*, 8391–8397, doi:10.1002/2015GL065746.
Udías, A., R. Madariaga, E. Buforn, D. Muñoz, and M. Ros (2012), The large Chilean historical earthquakes of 1647, 1657, 1730, and 1751 from contemporary documents, *Bull. Seismol. Soc. Am.*, *102*(4), 1639–1653.
Vigny, C., A. Socquet, S. Peyrat, J. C. Ruegg, M. Métois, R. Madariaga, S. Morvan, M. Lancieri, R. Lacassin, and J. Campos (2011), The 2010 M_w 8.8 Maule megathrust earthquake of central Chile, monitored by GPS, *Science*, *332*(6036), 1417–1421.
Wang, K., Y. Hu, M. Bevis, E. Kendrick, R. Smalley, R. B. Vargas, and E. Lauría (2007), Crustal motion in the zone of the 1960 Chile earthquake: Detangling earthquakecycle deformation and forearc-sliver translation, *Geochem. Geophys. Geosyst.*, *8*, Q10010, doi:10.1029/2007GC001721.
Wang, K., Y. Hu, and J. He (2012), Deformation cycles of subduction earthquakes in a viscoelastic Earth, *Nature*, *484*(7394), 327–332.
Weiss, J. R., et al. (2016), Isolating active orogenic wedge deformation in the southern Subandes of Bolivia, *J. Geophys. Res. Solid Earth*, *121*, 6192–6218, doi:10.1002/2016JB013145.
Wesson, R. L., D. Melnick, M. Cisternas, M. Moreno, and L. L. Ely (2015), Vertical deformation through a complete seismic cycle at Isla Santa Maria, Chile, *Nat. Geosci.*, *8*(7), 547–551.